Journal of Solid State Chemistry **165,** 324–333 (2002)
doi:10.1006/jssc.2002.9544, available online at http://www.idealibrary.com on IDEAL®

The Crystal Structure of $Bi_2PbMnO_4(PO_4)_2$, a Member of a New Solid Solution Series in the Bi–Pb–Mn–P Oxide System

Olivier Cousin,* Marielle Huve,† Pascal Roussel,† Olivier Perez,‡ and Hugo Steinfink*,[1]

*Texas Materials Institute and Department of Chemical Engineering, University of Texas, Austin, Texas 78712; †Laboratoire de Cristallochimie et Physicochimie du Solide, UMR CNRS 8012, ENSCL, BP 108, 59652 Villeneuve d'Ascq Cedex, France; and ‡Laboratoire CRISMAT-ISMRa, UMR CNRS 6508, 14050 Caen Cedex, France

Received August 7, 2001; in revised form February 5, 2002; accepted February 15, 2002

Single crystals of a new oxyphosphate were found while exploring the Bi–Pb–Mn–P oxide phase diagram. The reaction product from a mixture of Bi_2O_3, PbO, MnO_2, and $(NH_4)_2HPO_4$ in the ratio 1:1:2:2 displayed several phases including a Bi-rich phase with the approximate composition $(Bi_{3-x}Pb_x)MnP_2O_y$ and a Pb-rich phase with the approximate composition $(Bi_xPb_{4-x})MnP_3O_y$. A single crystal of the Bi-rich phase was selected. The title compound is tetragonal, $P\bar{4}2_1c$, $a = 13.275(3)$ Å, $c = 5.500(2)$ Å, $Z = 4$. The structure refinement converged to $R1 = 0.0442$. On the basis of the X-ray diffraction refinement, the formula is $Bi_2PbMnP_2O_{12}$. The crystal is an inverse twin. Electron diffraction revealed that the X-ray diffraction lattice parameters are from a subcell and the unit cell is $2a_{sub}$, $2b_{sub}$, $3c_{sub}$. The detailed study of reciprocal space, reconstructed from observations made using single-crystal electron diffraction data, leads us to an apparent wave vector $q^* = \frac{1}{2}a^* + \frac{1}{2}b^* + \frac{1}{3}c^*$, compatible with the Bravais lattice $4/mmmP(\frac{1}{2}\ \frac{1}{2}\ \gamma)$. However, this choice leads to forbidden reflections, e.g. $h00$, $h = 2n + 1$, due to the presence of a 2_1 axis. An assumption that the crystal consists of a modulated, twinned orthorhombic structure with space group $Ccc2$ based on the cell $\sqrt{2}a$, $\sqrt{2}a$, c leads to a modulation vector $q^* = a^* + \gamma c^*$. The (3 + 1)-dimensional Bravais lattice becomes $mmmC(10\gamma)$ and the super space group is $Ccc2(10\gamma)$. The refinement of the single crystal X-ray diffraction data based on $Ccc2$ consisting of two 90° twin domains led, as expected, to the identical result as the refinement in $P\bar{4}2_1c$.

The crystal structure was determined from the X-ray diffraction intensities based on the subcell and hence represents an averaged structure. The PO_4 radical can be present in two orientations. Pb occupies only $\frac{1}{2}$ of the crystallographic 8*e* positions. The Pb atoms bond through oxygen atoms from PO_4 to form a ring, creating channels parallel to *c*. Manganese and oxygen are present within the channels but the average structure prevents the determination of their location with certainty. Valence bond sums show that lead is tetravalent. The oxygen content requires tetravalent manganese. © 2002 Elsevier Science (USA)

INTRODUCTION

The exploration of the crystal chemistry and physical properties of the pseudoternary Bi–*M*–*X* and quaternary Bi–Pb–*M*–*X*, *M* = transition metals, *X* = P, V, As, oxide systems have been very extensive after the discovery that $Bi_4V_2O_{11}$ was a very good oxygen ion conductor (1). Recent studies of the system Bi–Pb–Mn–P–O led to the discovery of a cubic phase with composition $BiMn_6PO_{12}$ (2). The reaction product contained at least one other unknown phase characterized by brown, irregular crystals that were shown to be tetragonal. Quantitative X-ray energy dispersive analyses (EDX) on these crystals indicated that two separate solid solutions existed. A Bi-rich phase with the approximate composition $(BiPb)_3MnP_2O_x$, and a Pb-rich phase with the approximate composition $(BiPb)_4MnP_3O_x$. We selected one of the single crystals for X-ray diffraction analysis and report here the crystal structure of the Bi-rich phase.

EXPERIMENTAL

During the exploration of the ternary Bi–Mn–P oxide system, single crystals of an orthorhombic phase were observed. The preliminary crystal structure solution showed extensive atomic disorder and a chemically reasonable structure could not be extracted. Lead was introduced into the reaction mixture as a partial replacement for Bi or Mn in the hope that a modified structure will be formed without the severe atomic disorder. A mixture of analytical-grade Bi_2O_3, PbO, MnO_2, and $(NH_4)_2HPO_4$ in the ratio 1:1:2:2 was heated progressively to 800°C. The X-ray powder diffraction pattern of the product did not show the expected peaks from the orthorhombic phase. This product was then heated in a gold crucible above the melting point of 875°C. After 2 h at 875°C, the product was cooled to room temperature at 1.5°C/h. Two kinds of morphologies were observed; a few black broken cubes identified as $BiMn_6PO_{12}$ (2) and

[1] To whom correspondence should be addressed.

0022-4596/02 $35.00

TABLE 1
Crystal Data and Structure Refinement for $Bi_2PbMnP_2O_{12}$

Formula from refinement	Bi8.0 Mn5.46 O49.5 P8.0 Pb4.2
Formula	$Bi_2PbMnP_2O_{12}$
Formula weight	934
Temperature	293(2) K
Wavelength	0.71073 Å
Crystal system	Tetragonal
Space group	$P\bar{4}2_1c$
Unit-cell dimensions (Å)	
a	13.275(3)
c	5.500(2)
Volume (A^3)	969.2
Z, Calculated density (g/cm^3)	4, 6.40
$F(000)$	1596
Twin matrix	−100/0−10/00−1
Inverse twin fraction	0.5
Absorption coefficient (mm^{-1})	55.19
Crystal sphere, radius (mm)	0.1
Absorption correction (min/max/ave)	0.0048/0.0216/0.0146
Theta range for data collection (deg)	2.17–31.90
Limiting indices	$-19 <= h <= 19$, $-19 <= k <= 19$, $0 <= l <= 8$
Reflections collected/unique	5095/1481 [R(int) = 0.0425]
Completeness to theta = 31.90	92.4%
Refinement method	Full-matrix least-squares on F^2
Data/restraints/parameters	1481/39/89
Goodness-of-fit on F^2	1.134
Final R indices [$I > 2$sigma(I)]	$R_1 = 0.0446$, w$R_2 = 0.0832$
R indices (all data)	$R_1 = 0.0529$, w$R_2 = 0.0859$
Absolute structure parameter	0(6)
Extinction coefficient	0.00133(10)
Largest diff. peak and hole (e A^{-3})	2.017 and −1.839

brown, irregular-shaped crystals. The latter were selected for EDX using a Philips CM30 transmission electron microscope equipped with an energy-dispersive spectrometer. The average composition from 13 crystals of the Bi-rich phase was $Bi_{0.74}Pb_{0.20}Mn_{0.41}P_{0.59}$ calculated on the basis that Mn + P = 1. The average composition of the Pb-rich phase based on seven analyses was $Bi_{0.28}Pb_{0.57}Mn_{0.32}P_{0.68}$.

A Bi-rich single crystal was selected, ground into a sphere of about 0.2 mm diameter, and was mounted on a single-crystal CAD 4 automatic diffractometer. The data collection and results of the refinements are shown in Table 1. The diffraction symmetry was 4/*mmm*, the diffraction symbol 4/*mmmP*-/-2_1c leads to the unique space group $P\bar{4}2_1c$. The structure was solved using the Patterson superposition method and refined by least squares using the programs SHELXS and SHELXL (3). With the use of anisotropic displacement parameters for Bi, Pb, Mn1 and P the refinements converged to $R1 = 0.0446$ and Flack $x = 0.49$ indicating the presence of a twin. The inverse twinning matrix −100, 0−10, 00−1 was introduced, $R1$ remained the same and a BASF value of 0.50 indicated that equal parts of the twin are present. Eighty-nine parameters were refined using 39 restraints. The restraints were applied to the P–O and O–O bond lengths for two disordered tetrahedra centered on P with the additional requirement that the occupancies of their oxygen atoms add to unity. Electron diffraction patterns were obtained on a Jeol 200CX electron microscope. The material was crushed and dispersed on a holey carbon film deposited on a Cu grid. Because of the very high sensitivity of the sample to the electron beam, attempts to obtain high-resolution images were unsuccessful.

DISCUSSION

The atomic parameters and selected bond distances and angles are shown in Tables 2 and 3. The Bi site is fully occupied but the Pb site is only half occupied. There are two PO_4 tetrahedra centered on the P atom, P–O5, P–O8, P–O10, P–O11 and P–O3, P–O4, P–O7, P–O9. Only one of these is present in a given domain. The oxygen parameters of the first tetrahedron have high values of the displacement parameter indicative of some oscillatory motion. The average P–O bond distance is 1.34(2) Å. The oxygen atom displacement parameters of the second tetrahedron are much less and the average bond length, P–O 1.55(3) Å, is closer to the usual value. Similarly, only $\frac{1}{2}$ of the 8*e* Pb site is occupied so that a set of four Pb atoms is present in a given domain. The structure shown in Fig. 1 displays only one of the two possible PO_4 orientations and one set of four Pb positions. The Bi, Pb and PO_4 entities form a framework in which channels exist parallel to the

TABLE 2
Atomic Coordinates ($\times 10^4$) and Equivalent Isotropic Displacement Parameters ($A^2 \times 10^3$) for $Bi_2PbMnP_2O_{12}$

	sof	x	y	z	U(eq)
Bi	1	1393(1)	4919(1)	2349(1)	20(1)[a]
Pb	0.52(0)	1563(1)	2309(1)	2493(3)	24(1)[a]
Mn(1)	0.59(1)	0	0	2605(13)	50(2)[a]
Mn(2)	0.093(9)	0	0	0	16(4)
P	1	922(3)	−2107(5)	2273(18)	58(3)[a]
O(1)	$\frac{1}{2}$	0	$\frac{1}{2}$	4480(20)	21(3)
O(2)	1	1515(8)	3646(8)	4870(20)	23(3)
O(3)	0.59(3)	1044(16)	−1529(15)	−190(30)	40(6)
O(4)	0.59(3)	1882(14)	−2101(18)	3770(40)	41(6)
O(5)	0.45(3)	2320(30)	5130(30)	7440(100)	82(14)
O(6)	0.20(3)	0	0	$\frac{1}{2}$	60(20)
O(6′)	0.32(4)	0	0	1030(40)	3(5)
O(7)	0.59(3)	771(17)	−3298(14)	1360(40)	51(7)
O(8)	0.45(3)	750(40)	−1190(40)	3240(130)	240(50)
O(9)	0.59(3)	−26(14)	−1847(14)	3640(30)	37(5)
O(10)	0.45(3)	1720(30)	−2520(40)	3420(110)	150(30)
O(11)	0.45(3)	3820(50)	3030(60)	5090(80)	410(120)

[a] U(eq) is defined as one-third of the trace of the orthogonalized U_{ij} tensor. For all other atoms U(eq) is the isotropic value.

TABLE 3
Bond Lengths (Å), Angles (deg), and Valence Bond Values for $Bi_2PbMnP_2O_{12}$

Bi–O(2)	2.191(11)	0.77	Pb–O(11)#1	2.07(5)	0.46[a]	Mn(1)–O(6′)	0.86(2)
Bi–O(1)	2.193(7)	0.77	Pb–O(3)#6	2.104(9)	0.46[a]	Mn(1)–O(6)	1.317(7)
Bi–O(2)#1	2.344(11)	0.51	Pb–O(2)#1	2.145(12)	0.76	Mn(1)–Mn(2)	1.433(7)
Bi–O(1)#1	2.433(9)	0.40	Pb–O(2)	2.204(12)	0.65	Mn(1)–O(8)	1.90(5)
Bi–O(7)#2	2.51(2)	0.16[a]	Pb–O(9)#7	2.222(19)	0.31[a]	Mn(1)–O(8)#7	1.90(5)
Bi–O(7)#3	2.565(19)	0.14[a]	Pb–O(4)#8	2.25(2)	0.29[a]	Mn(1)–O(6′)#6	2.00(2)
Bi–O(5)#4	2.98(5)	0.05[a]	Pb–O(5)#1	2.29(4)	0.26[a]	Mn(1)–O(9)	2.518(19)
Bi–O(5)	3.07(5)	0.04[a]	Pb–O(4)#9	2.31(2)	0.23[a]	Mn(1)–O(9)#7	2.518(19)
Valence bond sum		2.84	Pb–O(10)#9	2.35(5)	0.22[a]	Mn(1)–Mn(1)#8	2.635(15)
			Pb–O(10)#8	2.70(6)	0.09[a]	Mn(1)–Mn(1)#6	2.865(15)
			Valence bond sum		3.70	Mn(2)–O(6′)#6	0.57(2)
						Mn(2)–O(6′)	0.57(2)
P–O(5)#11	1.31(4)		P–O(9)	1.507(16)		Mn(2)–Mn(1)#6	1.433(7)
P–O(8)	1.34(4)		P–O(4)	1.516(17)		Mn(2)–O(3)#10	2.46(2)
P–O(10)	1.35(4)		P–O(3)	1.565(18)		Mn(2)–O(3)#6	2.46(2)
P–O(11)#12	1.35(4)		P–O(7)	1.670(18)		Mn(2)–O(3)	2.46(2)
						Mn(2)–O(3)#7	2.46(2)
O(5)#11–P–O(8)	111.1(15)		O(9)–P–O(4)	115.5(10)			
O(5)#11–P–O(10)	111.3(15)		O(9)–P–O(3)	114.0(9)			
O(8)–P–O(10)	108.4(15)		O(4)–P–O(3)	112.3(9)			
O(5)#11–P–O(11)#12	110.4(16)		O(9)–P–O(7)	105.4(9)			
O(8)–P–O(11)#12	107.6(15)		O(4)–P–O(7)	105.6(9)			
O(10)–P–O(11)#12	107.9(15)		O(3)–P–O(7)	102.5(9)			

[a] Valence bond values for disordered oxygen atoms are multiplied by $\frac{1}{2}$. Symmetry transformations used to generate equivalent atoms: #1: $-y+\frac{1}{2}, -x+\frac{1}{2}, z-\frac{1}{2}$; #2: $y+\frac{1}{2}, x+\frac{1}{2}, z+\frac{1}{2}$; #3: $x, y+1, z$; #4: $x, y, z-1$; #5: $-y+\frac{1}{2}, -x+\frac{1}{2}, z+\frac{1}{2}$; #6: $-y, x, -z$; #7 $-x, -y, z$; #8: $-y, x, -z+1$; #9: $-x+\frac{1}{2}, y+\frac{1}{2}, -z+\frac{1}{2}$; #10: $y, -x, -z$; #11: $y-\frac{1}{2}, x-\frac{1}{2}, z-\frac{1}{2}$; #12: $-x+\frac{1}{2}, y-\frac{1}{2}, -z+\frac{1}{2}$; #13: $-x, -y+1, z$; #14: $y-\frac{1}{2}, x+\frac{1}{2}, z+\frac{1}{2}$; #15: $-y-\frac{1}{2}, -x+\frac{1}{2}, z+\frac{1}{2}$; #16: $y, -x, -z+1$; #17: $y, -x+1, -z+1$; #18: $x, y, z+1$; #19: $x, y-1, z$; #20: $-y+\frac{1}{2}, -x-\frac{1}{2}, z-\frac{1}{2}$; #21: $-y+1, x, -z+1$.

c-axis. There is continuous, variable electron density present in the channels, Fig. 2. High densities were assigned to Mn positions and lower densities to oxygen although mixed occupancies of Mn and O due to disorder are likely. The smearing of the electron density parallel to *c* makes it impossible to derive the correct locations of the Mn and O atoms in the channel or even the identity of an atom. The spatial parameters, site occupancies and atom types shown in Table 2 for atoms with 00*z* coordinates are qualitative. Matching the disordered atoms to yield reasonable bond lengths and environments is extremely uncertain; most "interatomic" distances for the atoms in the channel are unrealistic, Table 3.

As shown below the true unit cell is $2\mathbf{a}_{sub}$, $2\mathbf{b}_{sub}$, 3_{cub}. The stoichiometry of the compound derived from the subcell refinement is $Bi_8Pb_{4.18}Mn_{5.44}P_8O_{49.5}$. The values for Bi, Pb and P are reasonable but the Mn value needs to be examined in further detail. In the supercell eight channels are present. Short Mn–Mn distances are observed in $BaMnO_3$, 2.48 Å, (4) and 2.49 Å in $SrMnO_3$ (5). Thus, assuming a distance of about 2.5 Å, only six Mn can be present in each channel that is 16.5 Å in length in the supercell. The value of the refined site occupancy for Mn1 in site 4*c* of the subcell space group is 0.59 but cannot exceed 0.5 for full occupancy. Thus, there are two Mn per channel or four Mn in the subcell at a distance of about 2.75 Å. If Mn1 does not fully occupy its crystallographic site, i.e. some channels lack Mn1, then these channels could contain Mn2. The atomic disorder in the tunnels does not permit a definitive statement concerning the site occupancies. The refinement shows that there is sufficient electron density in the channels for four Mn atoms so that there is a high probability that, indeed, there are four Mn1 in the subcell and 48 in the supercell. Extra electron density arises from the oxygen environment around the Mn atoms. The oxygen spatial parameters cannot be extracted from the averaged structure. The most likely stoichiometry of this oxyphosphate is $Bi_2PbMnO_4(PO_4)_2$ or $Bi_{0.67}Pb_{0.33}Mn_{0.33}P_{0.67}$. This compound's formula is within the range of observed values.

The Bi atoms are in six-fold coordination to 2 O1, 2 O2, and 2 O5 or to 2 O1, 2 O2, and 2 O7 depending on which PO4 tetrahedron is present. A Bi atom is bonded to two neighboring Bi parallel to *c* by bridging O1 and O2 bonds. Parallel to *a* two Bi atoms are bridged by two O1 atoms. In addition, Bi atoms are bonded to either O5 or O7 that are part of a given PO_4 group, Fig. 3. The Bi–O form Aurivillius-type layers. The oxygen atoms, O5 and O11 of one PO_4 moiety and the 2 O2 bonded to Bi link to Pb to form

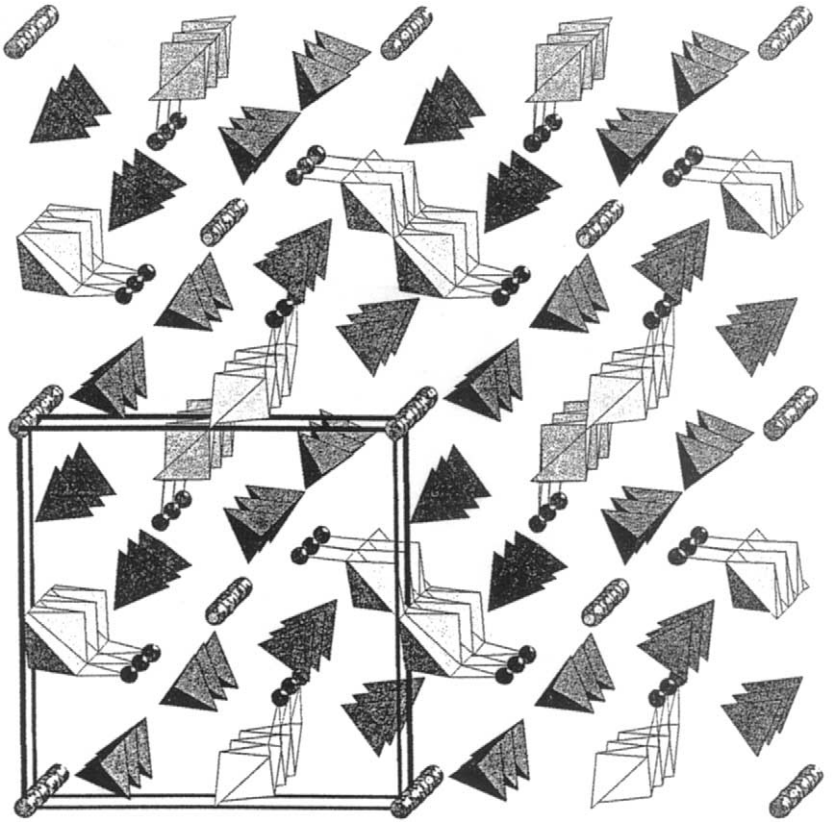

FIG. 1. The crystal structure of $Bi_2PbMnP_2O_{12}$. Only one of the two possible orientations of a PO_4 tetrahedron is shown and only one set of four Pb. Mn and oxygen atoms occupy the channels.

a framework structure containing channels parallel to *c*, Fig. 1. O5 and O11 from four separate PO4 radicals form a loop Pb–O11PO5–Pb–O11PO5–Pb–O11PO5–Pb O11PO5 Pb, Fig. 4, to link the four Pb atoms in a given domain. The channels contain Mn and O and because of the disorder the coordination polyhedra and atomic positions cannot be fixed with certainty. Mn^{4+} can occur in an octahedral (4, 5) or in a tetrahedral environment (6). A valence bond sum calculation with the program VaList showed that Bi was trivalent and Pb tetravalent (7).

It is evident that the structure solution is based on a subcell of the true cell. There was an initial hint of this because some very weak and infrequently occurring X-ray diffraction maxima could be seen in reciprocal space. Furthermore, the electron density in the channels evidently was due to the superposition of different atomic arrangements in the

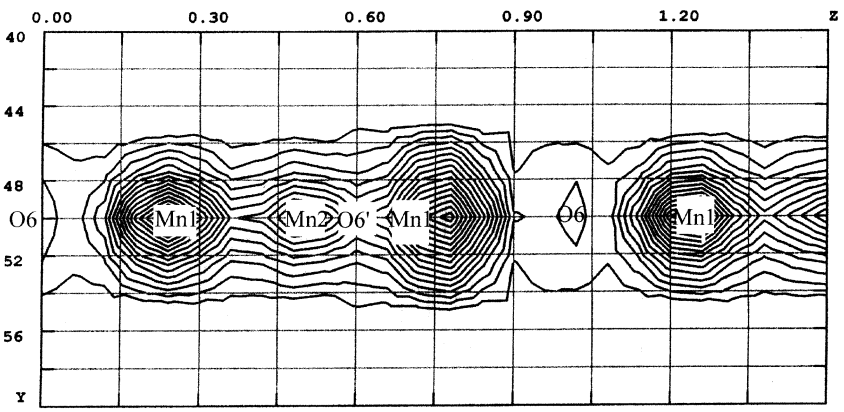

FIG. 2. The electron density in the channel at the $x = \frac{1}{2}$ level.

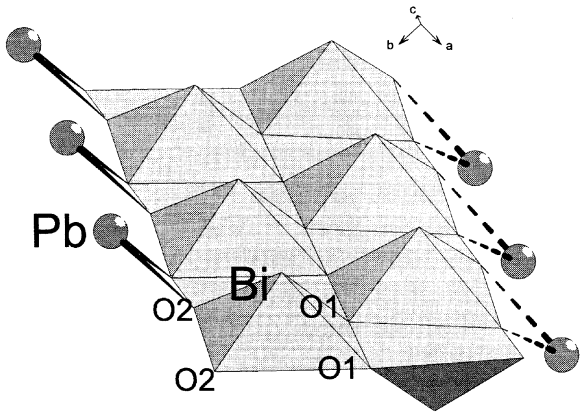

FIG. 3. The Bi–O layers and linkages to Pb.

channels before averaging. We therefore examined some of the crystals by electron diffraction.

ELECTRON DIFFRACTION

A selected area electron diffraction (SAED) study was performed to clarify the actual crystallographic symmetry. The electron diffraction patterns (EDP) collected for the zero order Laue zone (ZOLZ) for the [001], [010] and [110] zone axes are shown in Figs. 5a, b and c, respectively. The intense spots confirm the extinction conditions for the $P\bar{4}2_1c$ space group of the subcell used for the structural determination from the X-ray data. The $h00$, $h = 2n + 1$ and $00l$, $l = 2n + 1$ spots which appear on the EDP are due to double diffraction since they disappear upon tilting the sample. Thus, the (001) spot appears in the [010] orientation and not in the [110]. In addition to the intense spots, the [110] EDP, Fig. 5b, displays very diffuse streaks marked by arrows parallel to **a*** or **b***. Owing to the very weak intensity of these streaks, which correspond to a disorder in one direction of real space, they were not considered further. Nevertheless, perfect ordering can also occur as can be seen in Fig. 6 with the appearance of weak supplementary reflections. This ordering was observed in only one crystal among about 50.

A more interesting diffraction phenomenon is observed in the [110] EDP, Fig. 5c, in which additional intensity maxima (arrows) are observed between subcell diffraction spots, implying that the true direct space cell has dimensions $2\mathbf{a}_{sub}$, $2\mathbf{b}_{sub}$, $3\mathbf{c}_{sub}$. The extinction rules for the superstructure appear complex. In order to collect more information about the symmetry of this modulated structure, we examined the higher-order Laue zones (HOLZ).

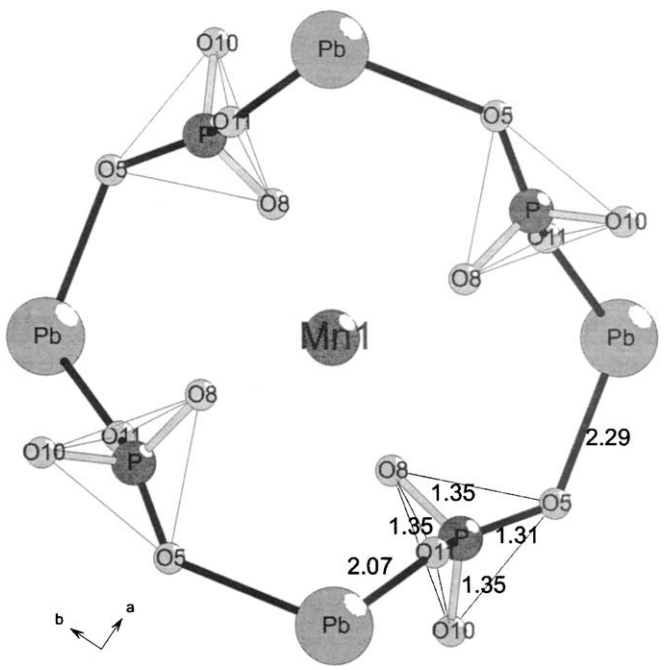

FIG. 4. View along [0 0 1] showing the ring forming the channel.

The [001]* Zone Axis

The tilting of the [001] EDP produces the higher-order Laue zones shown in Fig. 7. The tripling of the subcell c parameter is clearly shown by the two much weaker rows of reflections, labeled 1 and 2, interleaved between the much more intense rows of spots from the X-ray subcell labeled 0 and 3. The comparison between the ZOLZ and other Laue zones, in particular the comparison of the periodicity and shift between these different zones, provides the three-dimensional information required to identify the extinction rules of the superstructure. In agreement with the subcell space group $P\bar{4}2_1c$ no shift and difference of periodicity appears between the Laue zones 0 and 3 as well as for the -1 and $+1$ order Laue zones. The periodicity is the same for all the Laue zones. A half-shift is observed in both perpendicular directions of **a*** and **b*** between the 0 and 1 or -1 Laue zones and no shift is observed between the 1 and 2 Laue zones, Fig. 7. These observations lead to the schematic representation of the reciprocal space shown in Fig. 8 that represents a projection along **c*** of the reciprocal cell. The spots of the two additional Laue zones corresponding to the tripling of $\mathbf{c}_{sub}$ are placed on $\frac{1}{3}$ and $\frac{2}{3}$ of $\mathbf{c}^*_{sub}$ and shifted by $\frac{1}{2}$ of $\mathbf{a}^*_{sub}$ and $\frac{1}{2}$ of $\mathbf{b}^*_{sub}$.

The drawings shown in Fig. 8 provide a three-dimensional description so that they can be used to predict any other zone axis pattern. In order to verify the agreement between the information obtained from the different zone axes patterns, the predicted zone axis pattern was compared with the experimental one. The predicted projection of the [010] zone axis is obtained when one looks in the direction of arrow 1 of Fig. 8. The result is shown in Fig. 9. Comparison between the experimental ZOLZ, Fig. 5b, and

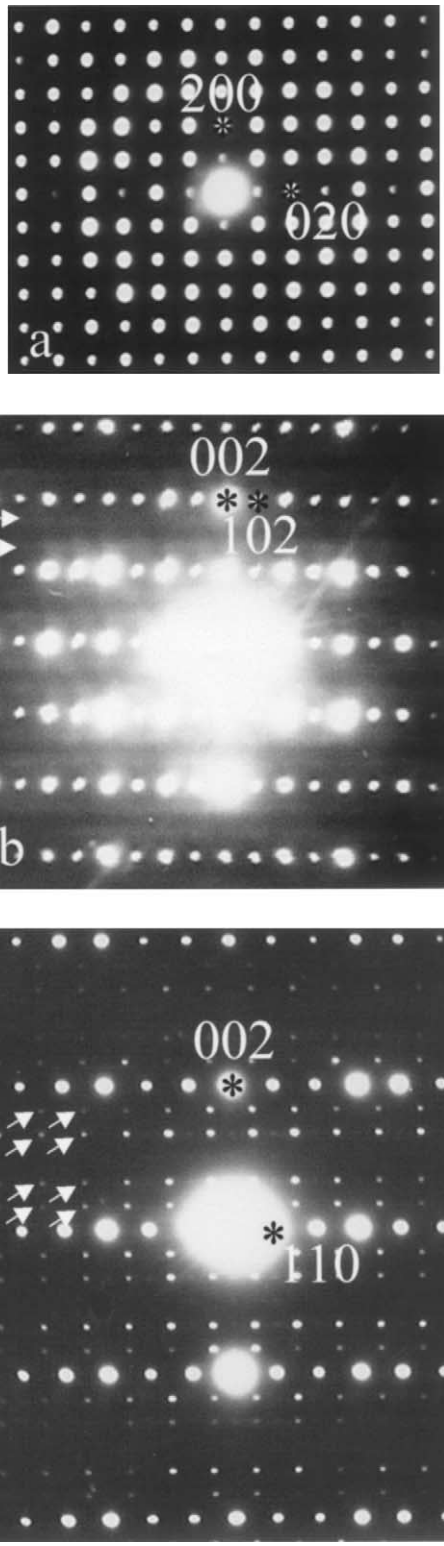

FIG. 5. Electron diffraction patterns (EDP) for the zero-order Laue zone (ZOLZ) for (a) [001], (b) [010] and (c) [110] zone axes. The intense spots confirm the extinction condition of the space group $P\bar{4}2_1c$ used for the structure determination. In addition, the latter two EDP display satellite reflections labeled by arrows.

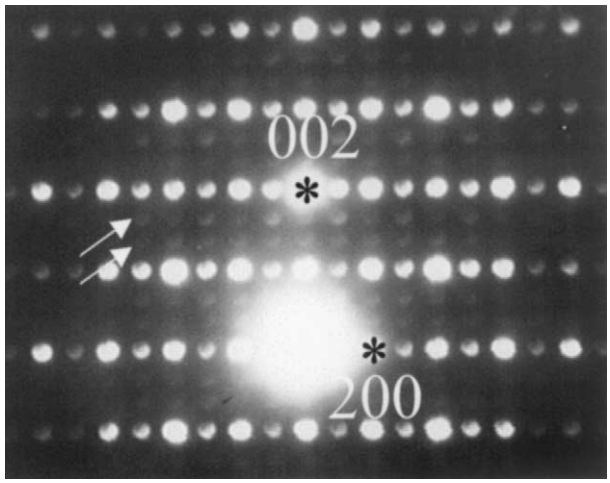

FIG. 6. Electron diffraction pattern for the [010] zone axis showing a rare crystal with ordering along **a***.

the predicted pattern, Fig. 9, shows good agreement. Careful examination of the patterns of the ZOLZ and FOLZ clearly shows that they are shifted by $\frac{1}{2}$ **a*** and $\frac{1}{3}$ **c***, Fig. 10.

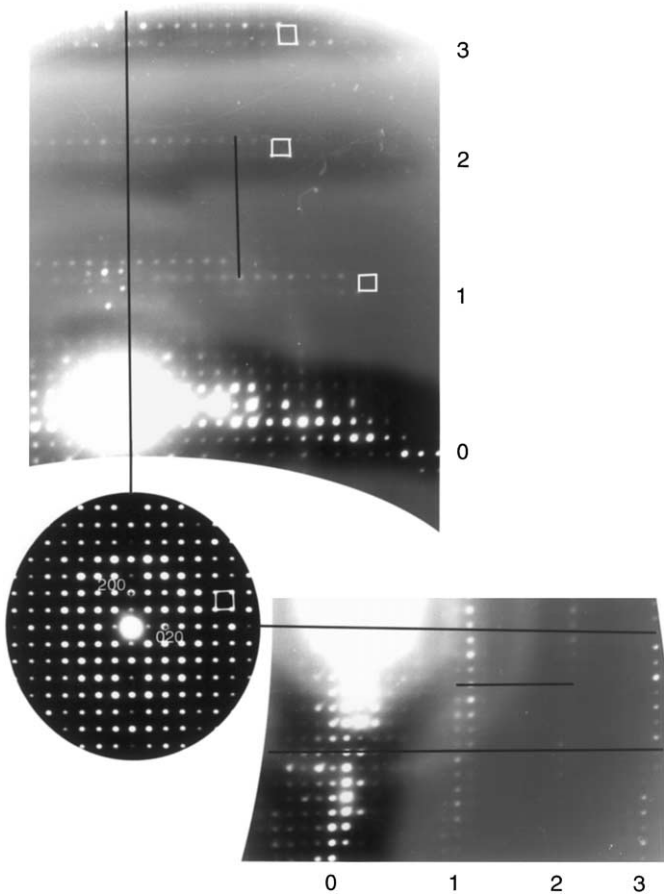

FIG. 7. Tilting of the [001] EDP exhibits the higher-order Laue zones. The numbers refer to the orders of the Laue zones.

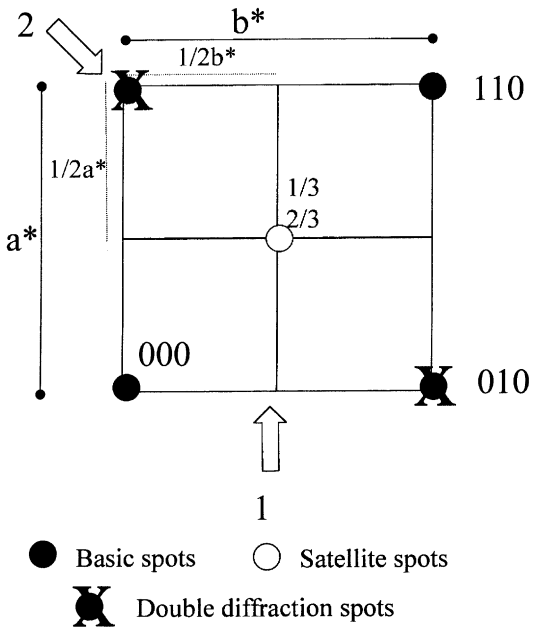

FIG. 8. Schematic representation of reciprocal space deduced from the [001] zone axis. EDP projected along [001].

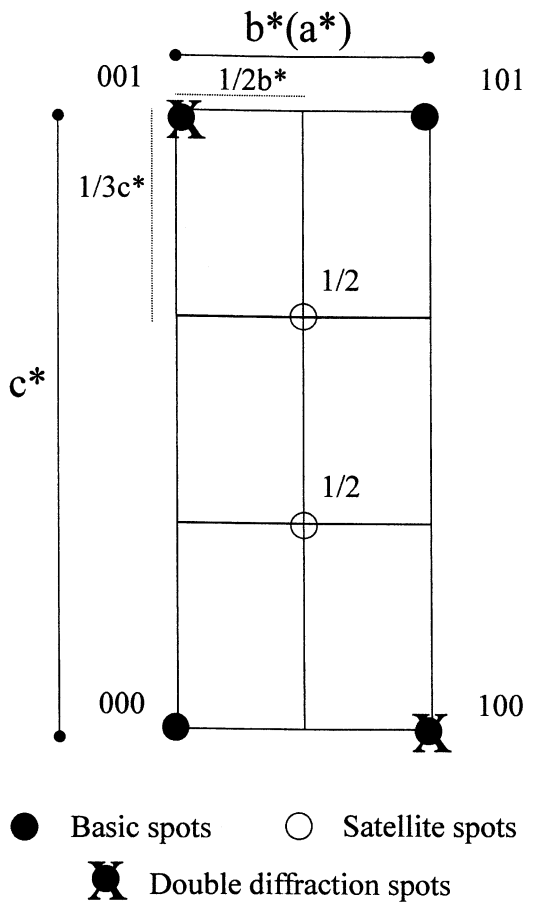

FIG. 9. Schematic representation of reciprocal space deduced from the schematic representation of reciprocal space in Fig. 8. Projection is along [100].

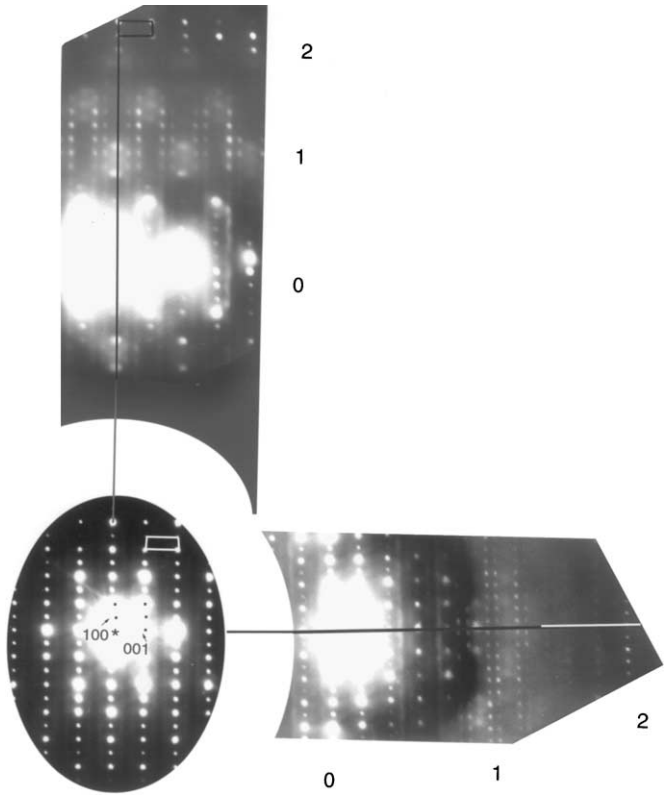

FIG. 10. The tilting of the [100] EDP exhibits the higher-order Laue zones. The numbers refer to the order of the Laue zone.

The predicted FOLZ, Fig. 9, and the experimental one, Fig. 10, can be superimposed. A similar comparison can be done for the [110] zone axis pattern. To obtain the predicted pattern one looks in the direction of arrow 2 in Fig. 8 and one can deduce Fig. 11 as the predicted pattern that agrees with the experimental pattern Fig. 5c.

SYMMETRY CONSIDERATIONS USING THE 4-D FORMALISM

In order to determine the space group of the supercell the approach described by van Smaalen was used (8). In this $(3 + N)$-dimensional formalism, modulated crystals can be considered as crystals with a classical three-dimensional periodicity that is periodically disrupted. The modulation is called commensurate, if dividing the period of the disruption by one of the 3-D basic crystal periodicities a rational number is obtained and incommensurate otherwise. The real, modulated structure can thus be described by its basic structure plus some distortion waves. Within this framework, a diffraction vector **H** can be written as

$$\mathbf{H} = h\mathbf{a}^* + k\mathbf{b}^* + l\mathbf{c}^* + m\mathbf{q}^*, \qquad [1]$$

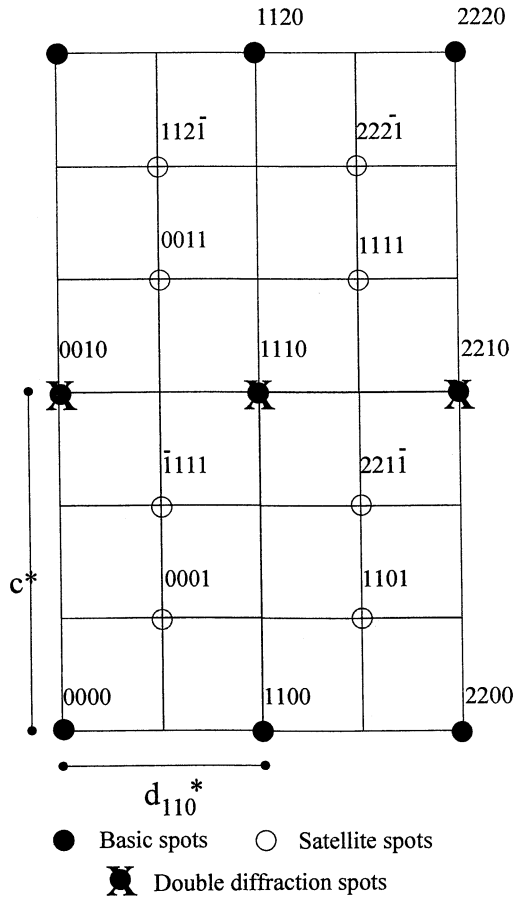

FIG. 11. Schematic representation of [110] reciprocal space deduced from the schematic representation of reciprocal space in Fig. 8. The agreement with the experimental pattern of Fig. 5c is perfect.

where h, k, l and m are integers and $\mathbf{q}^* = \alpha\mathbf{a}^* + \beta\mathbf{b}^* + \gamma\mathbf{c}^*$. Thus, the diffraction pattern consists of main and satellite reflections. The main and satellite reflections span a reciprocal lattice generated by **a***, **b***, **c*** and **a***, **b***, **c***, **q***, respectively; **a***, **b***, **c*** are the reciprocal parameters of the basic structure and **q*** the modulation wave vector.

The observed diffraction patterns can be elucidated in two different ways. We followed the steps recommended in Volume C of the International Tables for Crystallography to find the super-space group of a one-dimensional modulated structure (9). The Laue group P_L of the SAED diffraction pattern was determined as $(4/m)\,mm$. The parameters $a = 13.275$ Å, $b = 13.275$ Å, $c = 5.500$ Å define the basic structure and were used for indexing the main reflections. Therefore, to generate satellite reflections the wave vector $\mathbf{q}^* = \frac{1}{2}\mathbf{a}^* + \frac{1}{2}\mathbf{b}^* + \frac{1}{3}\mathbf{c}^*$, denoted by $(\frac{1}{2}\,\frac{1}{2}\,\gamma)$, compatible with the Bravais class $(4/m)\,mmP\,(\frac{1}{2}\,\frac{1}{2}\,\gamma)$, was chosen. The space group of the average structure $P\bar{4}2_1c$ is determined from the extinctions observed for the main reflections only. However, $P\bar{4}2_1c\,(\frac{1}{2}\,\frac{1}{2}\,\gamma)$ is not a possible super space group in $(3 + 1)$ dimensions, de Wolff *et al.* (10) and Table 9.8.3.5 (number 114.1) of International Tables for Crystallography, Volume C (9). The centering induced by the value of **q** is not compatible with the 2_1 screw axis. The 2_1 screw axis transforms $\mathbf{q} = (\frac{1}{2}\,\frac{1}{2}\,\gamma)$, into its symmetrical equivalent $\mathbf{q}' = (\frac{1}{2}\,-\frac{1}{2}\,-\gamma)$ and the second, mixed order satellite reflections obtained by combining **q** and **q**′, will correspond to a forbidden reflection, e.g. $h00$, $h = 2n + 1$. This contradicts the systematic extinction due to the screw axis, and hence this superspace group is not allowed.

Another approach to find a space group for the modulated structure led us to consider a lower symmetry for the basic structure of this compound. Three maximal non-isomorphic subgroups of $P\bar{4}2_1c$ can be used: tetragonal $P\bar{4}$ and two orthorhombic $P22_11$ and $P21c$, respectively, $P2_12_12$ and $Ccc2$ in the standard setting. The tetragonal $P\bar{4}$ subgroup was rejected because it does not explain the observed extinctions. As already shown for the space group $P\bar{4}2_1c$, the $P2_12_12$ space group cannot be considered because the 2_1 screw axes are not compatible with the **q** wave vector $(\frac{1}{2}\,\frac{1}{2}\,\gamma)$. Therefore, the orthorhombic subgroup $P21c$ in the setting **a**, **a**, **c**, or $Ccc2$ in the setting $\mathbf{a}\sqrt{2}$, $\mathbf{a}\sqrt{2}$, **c**, has been chosen. In an orthorhombic, pseudotetragonal structure the existence of 90° twin domains is a phenomenon which is very often observed. Assuming such oriented domains, then on the new basis $\mathbf{a}\sqrt{2}$, $\mathbf{a}\sqrt{2}$, **c** and the modulation wave vector $\mathbf{q}^* = \mathbf{a}^* + \gamma\mathbf{c}^*$, the whole diffraction pattern can be described. The $(3 + 1)$-dimensional Bravais class is $mmmC(10\gamma)$ and the super space group becomes $Ccc2(10\gamma)$. The **q*** vector can then be split into a rational component $\mathbf{q}_r = (1\,0\,0)$ and an irrational one $\mathbf{q}_i = (0\,0\,\gamma)$, with $\gamma = \frac{1}{3}$. The diffraction vector **H** of Eq. [1] can be

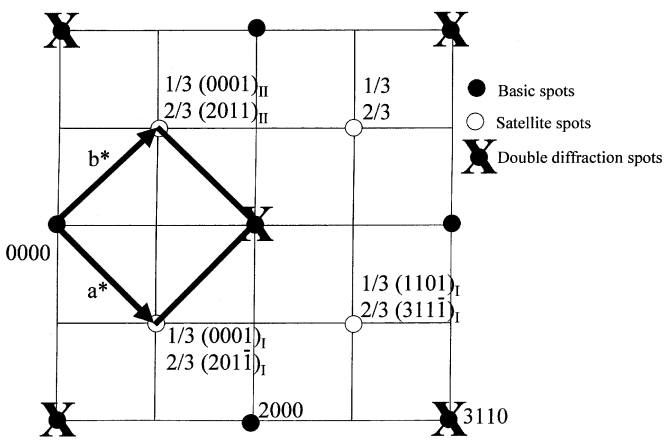

FIG. 12. [001] zone axis projection in the orthorhombic cell $\mathbf{a}\sqrt{2}$, $\mathbf{a}\sqrt{2}$, **c** with $\mathbf{q} = (10\frac{1}{3})$. Figure 8 is indexed with four integer indices *hklm*. **a*** and **b*** refer to this latter cell represented by the large dark lines $z = 0$. The satellite spots are generated by two 90° oriented domains labelled I and II.

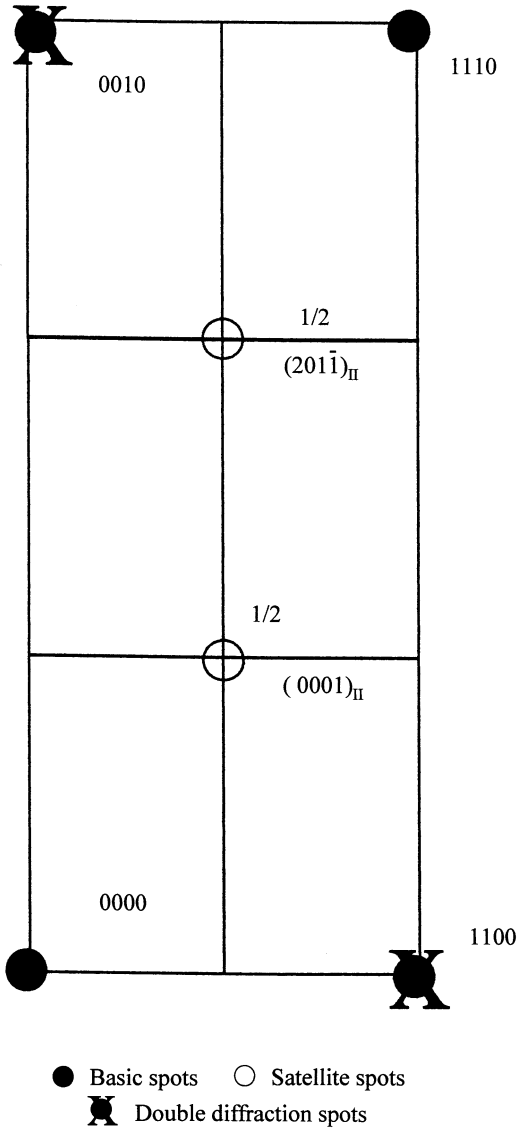

FIG. 13. The indexing of Fig. 9 with four integer indices *hklm* in the orthorhombic cell $\mathbf{a}\sqrt{2}, \mathbf{a}\sqrt{2}, \mathbf{c}$ and $\mathbf{q} = (10\frac{1}{3})$. Only one domain of the twin is shown in this pattern.

written as

$$\mathbf{H} = H\mathbf{a}^* + K\mathbf{b}^* + L\mathbf{c}^* + m\mathbf{q}_i \quad \text{with}$$

$$H = h + m,\ K = k,\ L = l.$$

Thus, in (3 + 1)-D space, the general condition for the *C* lattice translation is $H - m + K = 2n$ and the centering vector is $(\frac{1}{2}\frac{1}{2}0\frac{1}{2})$.

To validate this second hypothesis, a structural model for the average structure was determined in *Ccc*2 with two twin domains related y the matrix (0 1 0, -1 0 0, 0 0 -1).

The aim was not to determine a particular change with the tetragonal symmetry but rather to propose a symmetry compatible both with the basic structure and the observation of satellite reflections. Indeed, no information about the symmetry lowering is available in the X-ray diffraction data set. The main reflections of the different domains are perfectly superimposed. As already mentioned, the satellite reflections that belong to only one domain have very weak intensities and could not be collected using a standard X-ray source. We have verified that the same structure can be generated using $P\bar{4}2_1c$ and *Ccc*2, the same types of disorder occur during the refinement. The reliability factors reached in both symmetries are similar. Therefore, the super space group $Ccc2(10\gamma)$ is compatible with the modulated phase $Bi_8Pb_4Mn_4P_8O_{48}$.

Considering this latter symmetry, the EDP have been indexed without any problem in the cell $\mathbf{a}\sqrt{2}, \mathbf{a}\sqrt{2}, \mathbf{c}, \mathbf{q}^* = (10\frac{1}{3})$, in the superspace group $Ccc2(10\gamma)$, Figs. 12–14. The large dark lines in Fig. 12 indicate the "new" cell and the

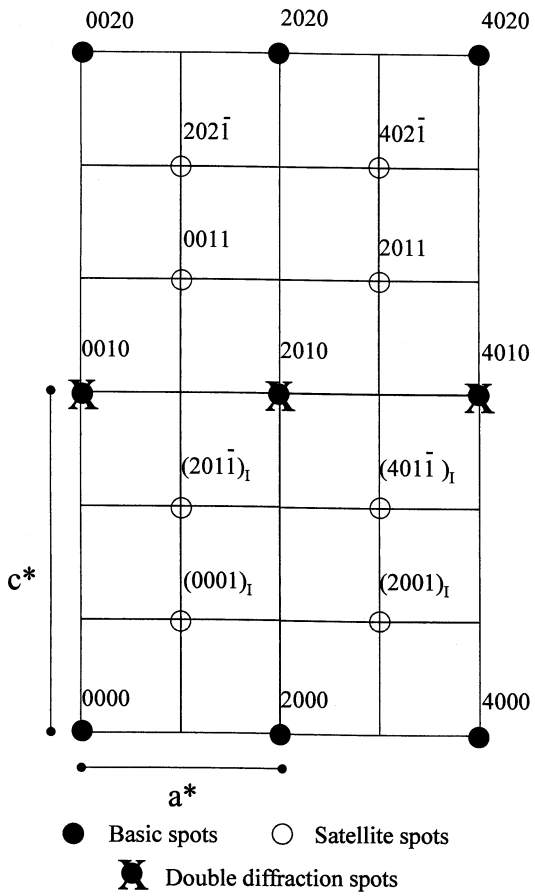

FIG. 14. The indexing of Fig. 11 with four integer indices *hklm* in the orthorhombic cell $\mathbf{a}\sqrt{2}, \mathbf{a}\sqrt{2}, \mathbf{c}$ and $\mathbf{q} = (10\frac{1}{3})$. The [010] zone axis projection exhibits satellites of domain I (defined in Fig. 12). The [100] ZAP is identical but shows satellites of domain II.

satellite spots are generated by two 90° oriented domains labelled I and II. Unfortunately, as already mentioned in the experimental part, the sample was very sensitive to the electron beam and high-resolution images that could have proved the existence of these domains, could not be obtained.

CONCLUSION

A new oxyphosphate with formula $Bi_2PbMnO_4(PO_4)_2$ has been synthesized, isolated and characterized by single-crystal X-ray diffraction and selected area electron diffraction methods. The average structure has been solved in the tetragonal space group $P\bar{4}2_1c$ using only main reflections since satellites reflections were not observable using our X-ray source. Electron diffraction revealed that the lattice parameters measured by X-ray diffraction comes from a subcell, whereas the true unit cell is $2\mathbf{a}_{sub}$, $2\mathbf{b}_{sub}$, $3\mathbf{c}_{sub}$. Symmetry considerations, using the 4-D formalism, lead us to conclude that even if the average, disordered, structure can be described in a tetragonal space group, the true modulated structure cannot be accounted for with such a symmetry. However, the orthorhombic superspace group $Ccc2(10\gamma)$, a subgroup of the tetragonal group, has been shown to be compatible with all our observations. This approach led us to discriminate between an orthorhombic twinned structure and a tetragonal one. Data obtained with synchrotron radiation would have provided the necessary satellite reflections to solve the modulated structure.

ACKNOWLEDGMENTS

O. C. and H. S. gratefully acknowledge the support of the R. A. Welch Foundation of Houston, TX. The authors appreciate useful discussions with Dr. Olivier Mentré, LCPS, Villeneuve d'Ascq, France and with Prof. Dominique Grebille, CRISMAT, Caen, France.

REFERENCES

1. J. C. Boivin and G. Mairesse, *Chem. Mater*. **10,** 2870 (1998).
2. O. Cousin, O. Mentre, M. Huve, and F. Abraham, *J. Solid State Chem.* **157,** 123 (2001).
3. G. M. Sheldrick, "SHELXS 97-2, a program for automatic solution of crystal structures" and "SHELXL 97-2, a program for crystal structure refinement." University of Göttingen, Germany 1997 as incorporated in L. J. Farrugia, WinGX v. 1.64.00 *J. Appl. Crystallogr*. **32,** 837 (1999).
4. Ph. Boullay, M. Hervieu, Ph. Labbe, and B. Raveau, *Mater. Res. Bull.* **32,** 35 (1997).
5. K. Kuroda, N. Ishizawa, N. Mizutani, and M. Kato, *J. Solid State Chem.* **38,** 297 (1981).
6. U. Delicat, S. F. Radaev, M. Tromel, P. Behrens, Y. F. Kargin, and A. A. Mar'in, *J. Solid State Chem.* **110,** 66 (1994).
7. A. S. Wills and I. D. Brown, "Program *VaList*." CEA, France, 1999.
8. S. van Smaalen, *Acta Crystallogr. A* **43,** 202 (1987).
9. A. J. C. Wilson, Ed., "International Tables for Crystallography," Vol. C. Kluwer Academic Publishers, Dordrecht, 1992.
10. P. M. de Wolff, T. Janssen, and A. Janner, *Acta Crystallogr. A* **37,** 625 (1981).